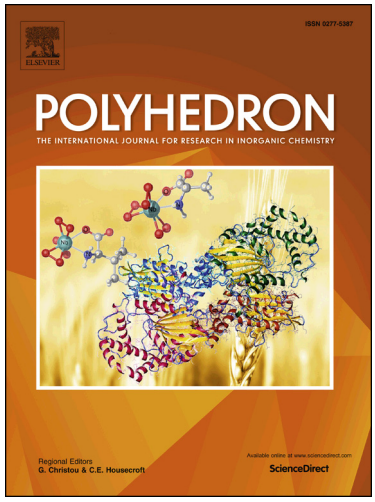

Tri- (M = Cu^{II}) and hexanuclear (M = Ni^{II}, Co^{II}) heterometallic coordination compounds with ferrocene monocarboxylate ligands: Solid-state structures and thermogravimetric, electrochemical and magnetic properties

Karoline Müller, Marcus Korb, Changhyun Koo, Rüdiger Klingeler, Dominique Miesel, Alexander Hildebrandt, Tobias Rüffer, Heinrich Lang

PII: S0277-5387(17)30598-3
DOI: https://doi.org/10.1016/j.poly.2017.09.021
Reference: POLY 12831

To appear in: *Polyhedron*

Received Date: 2 May 2017
Accepted Date: 14 September 2017

Please cite this article as: K. Müller, M. Korb, C. Koo, R. Klingeler, D. Miesel, A. Hildebrandt, T. Rüffer, H. Lang, Tri- (M = Cu^{II}) and hexanuclear (M = Ni^{II}, Co^{II}) heterometallic coordination compounds with ferrocene monocarboxylate ligands: Solid-state structures and thermogravimetric, electrochemical and magnetic properties, *Polyhedron* (2017), doi: https://doi.org/10.1016/j.poly.2017.09.021

Tri- (M = Cu^{II}) and hexanuclear (M = Ni^{II}, Co^{II}) heterometallic coordination compounds with ferrocene monocarboxylate ligands: Solid-state structures and thermogravimetric, electrochemical and magnetic properties

Karoline Müller,[a] Marcus Korb,[a] Changhyun Koo,[b] Rüdiger Klingeler,[b,c] Dominique Miesel,[a] Alexander Hildebrandt,[a] Tobias Rüffer,*[a] and Heinrich Lang[a]

[a] *Technische Universität Chemnitz, Faculty of Natural Science, Institute of Chemistry, Inorganic Chemistry, D-09107 Chemnitz, Germany*

[b] *Kirchhoff Institute of Physics, Heidelberg University, D-69120, Heidelberg, Germany*

[c] *Center for Advanced Materials (CAM), Heidelberg University, Heidelberg, Germany*

ABSTRACT

The synthesis and characterization of the hexanuclear $[M_2(\kappa O\text{-}O_2CFc)_2(\mu\text{-}O_2CFc)_2(\mu\text{-}H_2O)(\kappa^2 N,N'\text{-tmeda})_2]$ (M^{II} = Ni, **5**; Co, **6**; Fc = ferrocenyl, $(\eta^5\text{-}C_5H_4)(\eta^5\text{-}C_5H_5)Fe$; tmeda = *N,N,N',N'*-tetramethylethylendiamine) and the trinuclear $[Cu(\kappa^2 N,N'\text{-tmeda})(\kappa^2 O,O'\text{-}O_2CFc)_2]$ (**7**) coordination compounds are described. Compounds **5** – **7** were prepared by the consecutive reaction of ferrocene carboxylic acid ($FcCO_2H$; **1**) with $[^nBu_4N]OH$ followed by treatment of *in situ* formed $[^nBu_4N][FcCO_2]$ with the metal salts $[M(tmeda)(NO_3)_2]$ (M = Ni, **2**; Co, **3**; Cu, **4**). The structures of **5** – **7** in the solid state were determined by single crystal X-ray diffraction analysis. Isostructural **5** and **6** crystallise in the triclinic $P\bar{1}$ (**5**) and in the monoclinic space group $P2_1/n$ (**6**). The two M^{II}(tmeda) entities of **5** and **6** with M^{II} = Ni, Co, respectively, are *syn,syn*-bridged by two $FcCO_2^-$ functionalities and one μ-bridging water

molecule. Additionally, two $FcCO_2^-$ ligands are *κO*-coordinated to each M^{II} ion to form octahedral MN_2O_4 coordination setups. A related MN_2O_4 coordination setup is observed for **7** as well, whereby the Cu^{II} ion is coordinated by two O_2CFc and one tmeda ligand. Electrochemical investigations reveal that all individual Fc units of **5** – **7** are oxidized separately. Thermogravimetric analysis showed that **5** and **6** start to decompose at 110 and 125 °C and thus at significantly lower temperatures compared to **7** (200 °C). The mass residues obtained after decomposition are composed of Fe_2O_3, $FeNi_3$ and $Fe_{0.64}Ne_{0.36}$ (**5**), Fe and Co_3O_4 (**6**) and Cu_2O and $CuFeO_2$ (**7**), as determined by powder X-ray diffraction analysis (PXRD). Thermal susceptibility measurements of **5** and **6** determined a weak antiferromagnetic coupling in **5** and **6** with J = 1.1 K and J = 1.9 K, respectively.

ARTICLE INFO

KEYWORDS

molecular structure, electrochemical studies, single crystal X-ray diffraction, thermogravimetry, powder X-ray diffraction, magnetic susceptibility

CONTACT

Supplemental data for this article can be accessed at…

1. Introduction

The discovery, that the electrical resistance of a magnetic device is tunable by modifying its magnetic texture, thus of the giant magneto-resistance (GMR) effect [1–4], manifested the beginning of the field of magneto-electronics or, in other words, of *Spintronics*. As comprehensively reviewed by Sanvito [5], the use of organic molecules for the construction

of GMR devices gave rise to the new field *Molecular Spintronics*. Basically, " … The general idea behind spintronics is that of detecting the response of spins to an external stimulus …" [5], whereby the "organic molecule" could be even a single molecule magnet. Following this idea we became interested in the possible interplay between complexes displaying both intervalence charge/transfer properties and single molecule magnetic properties. Our group reported frequently on the synthesis and electrochemical properties of novel charge-transfer compounds, considering especially ferrocenyl-containing coordination compounds [6–10].

Previously, we have reported the electrochemical and magnetic properties of the isostructural hexanuclear coordination compounds $[M_2(O_2CFcCO_2)_2(H_2O)(tmeda)_2]$ (M = Ni, **8**; M = Co, **9**). We demonstrated, that the two ferrocenyl units of both **8** and **9** were oxidized at significant different redox potentials and that **8** exhibits a small ferromagnetic (θ = 1.6 K) and **9** an antiferromagnetic Weiss temperature (θ = –14.5 K) [11]. Furthermore, and in the search for Ni^{II}-containing coordination compounds which decompose to pure metallic nickel we recently reported on $[Ni_2(\kappa O\text{-}O_2CH)_2(\mu\text{-}O_2CH)_2(\mu\text{-}H_2O)(\kappa^2 N,N'\text{-tmeda})_2]$ (**10**) [12]. The structure of **10** is closely related to the one of **8** and **9**, and we were surprised that **10** exhibits a weak intramolecular antiferromagnetic coupling (J = –7.8 K) together with an easy plane magnetic anisotropy.

In order to narrow further to materials in which the spins response to an external stimuli we aimed to replace the two O_2CFcCO_2 ligands of **8** and **9** by four $FcCO_2$ ligands as in $[M_2(\kappa O\text{-}O_2CFc)_2(\mu\text{-}O_2CFc)_2(\mu\text{-}H_2O)(\kappa^2 N,N'\text{-tmeda})_2]$ (M^{II} = Ni, **5**; Co, **6**). Here we report on the synthesis and solid state structures of **5** and **6** together with $[Cu(\kappa^2 N,N'\text{-tmeda})(\kappa^2 O,O'\text{-}O_2CFc)_{2\ 2}]$ (**7**). Furthermore, we describe the thermal and electrochemical properties of **5** – **7** and the results of susceptibility studies of **5** and **6**.

2. Experimental Section

2.1. Materials and measurements.

All reactions were carried out under an atmosphere of argon unless otherwise stated. Starting materials $Fc(CO_2H)$ (**1**) and $[M(tmeda)(NO_3)_2]$ (M = Ni (**2**), Co (**3**), Cu (**4**)) were prepared by published procedures [11,13]. Pyridine was dried with KOH, distilled under argon atmosphere and stored over molecular sieve 4 Å. Acetonitrile was purified by distillation from P_4O_{10}. Diethyl ether and dichloromethane were dried using a MBraun MP SPS-800 system (double column solvent filtration, working pressure 0.5 bar). The melting points were determined using a Gallenkamp MFB 595 010 M melting point apparatus. The elemental analyses were measured with a Thermo FlashEA 1112 Series instrument. IR spectra were measured using KBr pellets in the range of 400 – 4000 cm^{-1} with a Nicolet IR 200 spectrometer from Thermo Electron Corporation. For each spectrum 16 scans were measured at a resolution of 2 cm^{-1}. High-resolution mass spectra were recorded with a Bruker Daltonik microTOF-QII spectrometer. Thermal gravimetric measurements combined DSC measurements were performed with a Mettler Toledo TGA/DSC1 1600 System equipped with a MX1 balance. X-ray powder diffraction (PXRD) studies were performed with a STOE-STADI-P diffractometer with $CuK_{\alpha 1}$ = 1.540 Å in the range of 20 – 90 ° for 2θ. Electrochemical measurements were performed on 1.0 $mmol \cdot L^{-1}$ solutions of **5** – **7** in dichloromethane in a dried, argon-pulled cell at 25 °C with a Radiometer Voltalab PGZ 100 electrochemical workstation interfaced with a personal computer. $[^nBu_4N][B(C_6F_5)_4]$ (0.1 $mol \cdot L^{-1}$) was used as supporting electrolyte.

Spectroelectrochemical UV-Vis/NIR measurements of 1.0 mmol L^{-1} solution of **6** in anhydrous acetonitrile containing 0.1 mol L^{-1} of $[^nBu_4N][B(C_6F_5)_4]$ as the supporting electrolyte were performed in an OTTLE (= Optically Transparent Thin-Layer Electrochemical) [14] cell with a Varian Cary 5000 spectrophotometer at 25 °C.

The static magnetic susceptibility $\chi(T) = M(T)/B$ of **5** and **6** was measured by means of a Quantum Design MPMX XL-5 SQUID magnetometer. The measurements were done in the temperature range of T = 2 - 300 K and at B = 5 T and 1 T, respectively. In order to account for the contribution of the ligands, the temperature independent diamagnetic susceptibility of the coordination compounds as calculated by means of Pascal's constants has been subtracted from the experimental data [15].

Crystallographic studies. All data were collected with an Oxford Gemini S diffractometer. All structures were solved by direct methods using SHELXS-2013 and refined by full-matrix least-square procedures on F^2 using SHELXL-2013 [16]. All *non*-hydrogen atoms were refined anisotropically. All *C*-bonded hydrogen atoms were refined using a riding model. For further details cf. Table S1 and additional explanation (SI).

2.2. Synthesis of $[Ni_2(O_2CFc)_4(H_2O)(tmeda)_2]$ (5).

$FcCO_2H$ (**1**) (150 mg, 0.652 mmol) was suspended in acetonitrile (20 mL) and $[^nBu_4N]OH$ (0.42 mL, 0.652 mmol, 40% in water) was added in a single portion at ambient temperature. After stirring this solution for 20 min, a solution of $[Ni(tmeda)(NO_3)_2]$ (**2**) (97 mg, 0.326 mmol) in acetonitrile (10 mL) was added drop−wise. After stirring for 2 h the solution volume was reduced to 5 mL and stored over night at 5 °C. The obtained precipitate was filtered off and washed with cold acetonitrile (2 × 3 mL) and diethyl ether (2 × 3 mL). The solid was recrystallized in a mixture of acetonitrile and diethyl ether (ratio 3:5, *v*/*v*) and stored at 5 °C. After one week crystals suitable for crystallographic studies were obtained, filtered off, washed with cold diethyl ether (2 × 3 mL) and were dried in vacuum. Yield: 0.143 mg (68 % of **5** based on **1**). *Comment:* Crystals selected under an optical microscope for crystallographic characterisation were observed to become quickly brittle, which indicates loss of packing

solvent molecules. Note that crystallographic characterisation revealed a composition of [(**5**)$_2$(MeCN)$_3$(Et$_2$O)] (**5'**). The elemental analysis of **5** dried in vacuum confirmed the loss of the packaging solvent molecules (Anal. Calcd. for $C_{56}H_{72}N_4O_9Ni_2Fe_4$ (1285.96 g/mol, **5**; %): C, 52.30; H, 5.64; N, 4.36. Found: C, 51.98; H, 5.85; N, 4.34.), while material that was stored on air produced an elemental analysis which refers to **5** with an incorporation of one molecule of H_2O per molecule of **5**. M.p.: 175 °C. Anal. Calcd. for $C_{56}H_{74}N_4O_{10}Ni_2Fe_4$ (1303.97 g/mol, **5**·H_2O; %): C, 51.58; H, 5.72; N, 4.30. Found: C, 51.46; H, 5.80; N, 4.46. IR (KBr, cm^{-1}): 3096 (w), 3018 (w), 2903–2840 (m), 2794 (w), 2055 (w, br), 1617 (s), 1534 (w, br), 1473 (s), 1388 (s), 1359 (s), 1348 (m, sh), 1287 (w), 1187 (w), 1106 (w), 1024 (m), 957 (w), 802 (m), 773 (s). ESI–MS: *m*/*z* = 403.0732 $[M - Ni(tmeda)(O_2CFc)_3]^+$; 1035.1187 $[M - O_2CFc]^+$. Fig. S1 (SI) gives the IR spectra of **5** and **5**·H_2O and Figure S4 (SI) the ESI-MS spectrum of **5**.

2.3. Synthesis of [Co$_2$(O$_2$CFc)$_4$(H$_2$O)(tmeda)$_2$] (6).

Compound **6** was prepared according to the procedure reported for **5**. $FcCO_2H$ (**1**) (150 mg, 0.652 mmol) was reacted with [^{n}Bu$_4$N]OH (0.42 mL, 0.652 mmol; 40% in water) and [Co(tmeda)$(NO_3)_2$] (**3**) (94 mg, 0.33 mmol) in acetonitrile. After stirring for 2 h at ambient temperature the volume was reduced to 5 mL and stored over night at 5 °C. The formed precipitate was filtered and washed with acetonitrile (2 × 3 mL) and diethyl ether (2 × 3 mL). Crystals were obtained out of a mixture of acetonitrile and diethyl ether (ratio 3:5, *v*:*v*) containing **6** after partial evaporation of diethyl ether. Yield: 0.125 mg (60 % for **1**). M.p.: 195 °C (decomp.). Anal. Calcd. for $C_{56}H_{72}N_4O_9Co_2Fe_4$ (1286.44 g/mol; %): C, 52.28; H, 5.64; N, 4.36. Found: C, 52.37; H, 5.74; N, 4.25. IR (KBr, cm^{-1}): 3090 (w), 3012 (w), 2974 (w), 2907 – 2839 (m), 2788 (w), 2048 (w, br), 1612 (s), 1532 (w, br), 1472 (s), 1388 (s), 1359 (m), 1347 (m), 1283 (w), 1158 (w), 1106 (w), 1015 (m), 951 (w), 799 (m), 767 (m), 560 (m). ESI–MS:

m/*z* = 404.0660 [M – Co(tmeda)($O_2CFc)_3$]$^+$; 1037.1144 [M – O_2CFc]$^+$. Fig. S1 (SI) gives the IR spectrum of **6** and Fig. S5 (SI) gives the ESI-MS spectrum of **6**.

2.4. Synthesis of [(tmeda)Cu($O_2CFc)_2$] (7).

Compound **7** was prepared according to the procedure reported for **5**. $FcCO_2H$ (**1**) (150 mg, 0.652 mmol) was reacted with [^{n}Bu_4N]OH (0.42 mL, 0.652 mmol, 40% in water) and [Cu(tmeda)($NO_3)_2$] (**4**) (99 mg, 0.326 mmol) in acetonitrile. After stirring the reaction mixture for 1 h at ambient temperature, the precipitated solid was filtered and washed with diethyl ether (3 × 10 mL). Single crystals were obtained by slow diffusion of diethyl ether into a solution of dichloromethane containing **7** at ambient temperature. For purification the crystallisation procedure had to be carried out twice. Yield: 0.176 mg (84 % for **1**). M.p.: 230 °C (decomp.). Anal. Calcd. for $C_{28}H_{34}N_2O_4CuFe_2$ (637.82 g/mol; %): C, 52.73; H, 5.37; N, 4.39. Found: C, 52.43; H, 5.44; N, 4.20. IR (KBr, cm^{-1}): 3109 – 3086 (w, m), 2979 – 2803 (w, m), 1566 ($\nu_{asym}(CO_2)$, vs), 1467 ($\nu_{asym}(CO_2)$, s), 1385 ($\nu_{sym}(CO_2)$, s), 1385 ($\nu_{sym}(CO_2)$, s), 1354 (m, sh), 1336 (s), 1289 (w), 1180 (m), 1105 (m), 1021 (m), 1003 (w), 957 (w), 797 (s), 512 (m). ESI–MS: *m*/*z* = 408.0557 [M – O_2CFc]$^+$; 637.0510 [M]$^+$; 660.0408 [M + Na]$^+$. Fig. S1 (SI) gives the IR spectrum of **7** and Fig. S6 (SI) gives the ESI-MS spectrum of **7**.

3. Results and Discussion

3.1. Synthesis

The consecutive synthetic methodology to prepare **5** – **7** is shown in Scheme 1 and is analogous to our previous report [11]. The reaction of ferrocene monocarboxylic acid ($FcCO_2H$, **1**) with $[^nBu_4N]OH$ in a 1:1 molar ratio in acetonitrile afforded *in situ* generated $[^nBu_4N][FcCO_2]$, which upon treatment with the appropriate amount of the metal salts $[M(tmeda)(NO_3)_2]$ (M = Ni, **2**; Co, **3**; Cu, **4**) produced either discrete hexanuclear M_2Fe_4 $[M_2(O_2CFc)_4(H_2O)(tmeda)_2]$ (M = Ni, **5**; Co, **6**) or trinuclear $CuFe_2$ $[Cu(tmeda)(O_2CFc)_2$ (**7**) (Scheme 1).

Solids of **5** and **6** are soluble in most common organic solvents including diethyl ether and acetonitrile, while **7** is insoluble in polar solvents. After appropriate work-up **5** – **7** were isolated as yellow, orange or green solids, respectively (Experimental Section). Crystals of **5** were characterized as $[(\mathbf{5})_2(MeCN)_3(Et_2O)]$ (**5'**) while crystals of **6** do not any contain packing solvent.

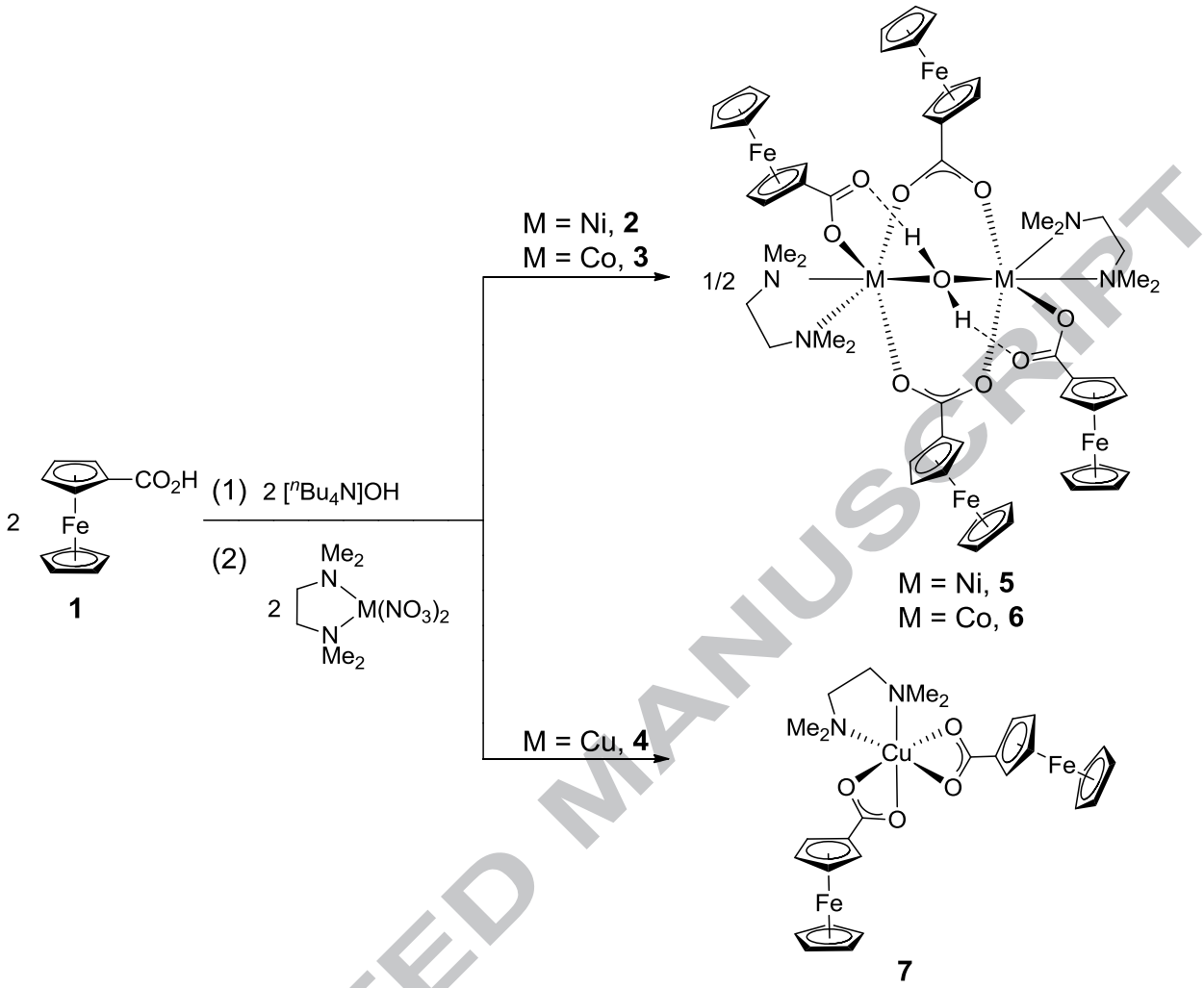

Scheme 1. Synthesis of **5** – **7** from **1** and [M(tmeda)$(NO_3)_2$] (M = Ni, **2**; M = Co, **3**; M = Cu, **4**).

3.2. IR spectroscopy

The IR spectra of **5** – **7** are shown in Fig. S1 (SI) and display similar spectral features for all three coordination compounds. For example, all spectra exhibit four intense $\nu(CO_2)$ vibrations in the region of 1300 – 1600 cm^{-1} due to the different binding motifs of the $FcCO_2$ ligands. Single crystal X-ray diffraction studies proved for isostructural **5** and **6** two κO–O_2CFc and two μ-O_2CFc bonded ligands (Scheme 1, Fig. 1). Generally, it is possible to distinguish between the different binding motifs of carboxylates by the intensities of the CO_2 stretching frequencies and the difference of the asymmetric (ν_{asym}) and symmetric (ν_{sym}) CO_2 vibrations ($\Delta\nu$, $\Delta\nu = \nu_{asym} - \nu_{ym}$; $\Delta\nu_{chelating}(CO_2) < \Delta\nu_{bridging}(CO_2) \leq \Delta\nu_{ionic}(CO_2) << \Delta\nu_{unidentate}(CO_2)$) [17,18].

However, we recently reported for the IR spectroscopic characterization of **10**, inclusive accompanying DFT calculations [12], that these common assigning rules are not precisely applicable. A related situation is observed for here reported **5** and **6** and thus it is not possible to assign unambiguously the $\nu_{asym}(CO_2)$ and $\nu_{sym}(CO_2)$ vibration modes. Another characteristic of both **5** and **6** is a very broad band at approximately 2000 cm^{-1}, which presents the OH vibration of the μ-bridging water ligand, as observed for **10** [12,19,20]. The significant shift of the OH vibration of **5**, **6** and **10** [12] to higher energies, when compared to free water, is based on the intramolecular hydrogen bonding between the μ-bridging water and the *kO*-bonded carboxylate ligands (Fig. 1) and is additionally verified by DFT calculations [17,19,21–23]. For **7** the presence of two asymmetrically k^2O,O'-bonded O_2CFc ligands was found (Scheme 1, Fig. 2). The respective $\nu(CO_2)$ absorptions of **7** are, compared to **5** and **6**, somewhat shifted to smaller wavenumbers (1565, 1466 ($\nu_{asym}(CO_2)$); 1385, 1336 ($\nu_{sym}(CO_2)$) cm^{-1}) (Experimental Section). The $\Delta\nu$ (180 and 130 cm^{-1}) agree with the observed binding motif of the O_2CFc ligands according to the literature [17,18].

3.3. The molecular structures of 5 – 7

The structures of 5 and 6: In case of **5'** the asymmetric unit of the centrosymmetric triclinic unit cell comprises two crystallographically independent molecules of **5**, denoted as **5A** (including Ni1 and Ni2) and **5B** (including Ni3 and Ni4). Such a phenomena is observed for **6** as well, as in case of **6** the asymmetric unit of the centrosymmetric monoclinic unit cell in $P2_1/n$ comprises two crystallographically independent molecules, denoted as **6A** (including Co1 and Co2) and **6B** (including Co3 and Co4). Related structural features of **5A**/**5B** and **6A**/**6B** compare well with each other and therefore all further discussion refer to **5A** and **6A** only. Thus, the molecular structures of **5A** and **6A** are presented in Fig. 1 and selected bond lengths and angles are summarized in Table 1.

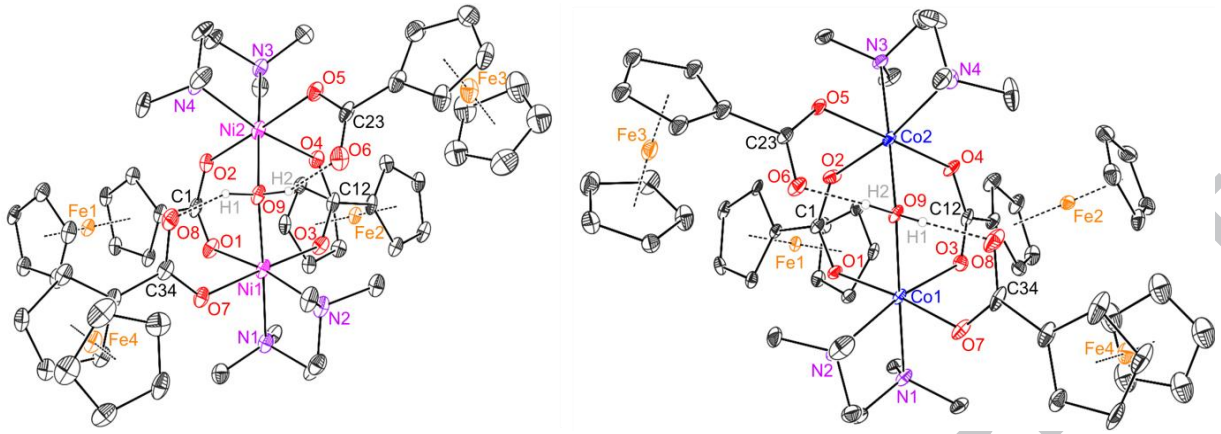

Fig. 1. ORTEP (25 % ellipsoid probability) of the molecular structures of **5A** (left) and **6A** (right). All *C*-bonded hydrogen atoms were omitted for clarity. Of disordered Fc units of **6A** only one atomic position is shown. Intramolecular hydrogen bonds and iron to geometrical centroid distances of C_5H_4 and C_5H_5 units were indicated by dotted lines.

Hexanuclear **5A** and **6A** (Fig. 1) belong to a family of Ni^{II}_2- [11,24–41] and Co^{II}_2-containing [11,19,24,31,41–64] coordination compounds possessing related bis(carboxylate)-1κO;2κO-bis(μ-carboxylate-1:2k^2O,O')-μ-aqua-1:2κ^2O cores. In this family the organic groups R of the carboxylate ligands O_2CR vary, as well as the nature of additional mono- or bidentate N-donor ligands coordinated to the metal ions. Thus, each metal atom of **5A**/**6A** is coordinated by the μ-aqua ligand, by two O-donor atoms of two μ-$FcCO_2$ ligands, by one O-donor atom of a κO-bonded $FeCO_2$ entity and by a κ^2N,N'-bonded tmeda unit, resulting in distorted octahedral MO_4N_2 setups. Accordingly, bond angles of *trans*-aligned donor atoms cover a range from 169.8 to 178.7 ° for **5A**, and 169.2 to 178.8 ° for **6A**, while those of *cis*-aligned donor atoms cover a range from 84.4 to 96.8 ° for **5A**, and 82.1 to 98.8 ° for **6A** (Table 1).

Bond lengths and angles of **5A** and **6A** compare well with related values described for already crystallographically characterized analogous coordination compounds. To verify this, selected structural features of coordination compounds of the type $[M_2(O_2CFc)_4(H_2O)(tmeda)_2]$ (M = Ni, [11,24–41],[65] Co [11,19,24,31,41–64]) were searched with the Cambridge Structural Database (CSD, version 5.37, 02/2016) and were compared with **5A** and **6A** as described in the SI. In summary it can be stated, that isostructural **5A** and **6A** show no structural

peculiarities and compare well to already described analogous coordination compounds. There is a final remark: Although **5A** and **6A** are isostructural, they are not isomorphic as their crystallographic data (unit cell, space group) differ. In Fig. S8 (SI) an overlay of the cores of both coordination compounds is displayed revealing minor deviation, although the orientation of the terminal Fc substituents differs. That proves that the Fc substituents can freely rotate in solution.

Table 1. Selected bond lengths [Å] and angles [°] of **5A**, **6A** and **7**. [a)]

Bond lengths							
	5A	**6A**		**5A**	**6A**		**7**
M1–O1	2.033(4)	2.045(5)	M2–O2	2.026(4)	2.040(5)	Cu1–N1	2.034(3)
M1–O3	2.016(4)	2.052(5)	M2–O4	2.020(4)	2.065(5)	Cu1–N2	2.034(3)
M1–O7	2.094(4)	2.063(18)	M2–O5	2.064(4)	2.099(5)	Cu1–O1	2.550(2)
M1–O9	2.088(4)	2.125(5)	M2–O9	2.077(4)	2.113(5)	Cu1–O2	1.947(2)
M1–N1	2.158(5)	2.221(6)	M2–N3	2.161(5)	2.222(6)	Cu1–O3	1.953(2)
M1–N2	2.179(5)	2.257(6)	M2–N4	2.180(4)	2.215(6)	Cu1–O4	2.594(2)
C1–O1	1.253(6)	1.267(8)	C1–O2	1.251(7)	1.242(8)	C1–O1	1.245(4)
C12–O3	1.268(7)	1.249(8)	C12–O4	1.271(8)	1.277(9)	C1–O2	1.286(4)
C23–O5	1.277(7)	1.249(8)	C23–O6	1.264(7)	1.252(8)	C12–O3	1.285(4)
C34–O7	1.276(7)	1.256(18)	C34–O8	1.252(7)	1.256(19)	C12–O4	1.248(4)
Fe1–D1[b)]	1.644(3)	1.651(4)	Fe1–D2[b)]	1.643(3)	1.657(4)	Fe1–D1[c)]	1.647(2)
Fe2–D3[b)]	1.642(3)	1.652(4)	Fe2–D4[b)]	1.644(3)	1.649(4)	Fe1–D2[c)]	1.647(2)
Fe3–D5[b)]	1.637(2)	1.639(4)	Fe3–D6[b)]	1.641(3)	1.666(4)	Fe2–D3[c)]	1.648(2)
Fe4–D7[b)]	1.628(4)	1.630(4)	Fe4–D8[b)]	1.649(4)	1.632(4)	Fe2–D4[c)]	1.660(2)
Bond angles							
M1–O9–M2	116.49(15)	116.4(2)				N1–Cu1–N2	86.71(12)
O1–M1–O3	93.59(15)	95.4(2)	O2–M2–O4	91.66(16)	89.9(2)	O2–Cu1–O3	92.31(10)
O1–M1–O7	177.48(16)	174.2(12)	O2–M2–O5	88.61(16)	87.6(2)	O2–Cu1–N2	162.63(10)
O1–M1–O9	92.67(15)	91.90(18)	O2–M2–O9	92.78(14)	93.62(19)	O3–Cu1–N1	167.38(11)
O3–M1–O9	92.74(15)	89.75(19)	O4–M2–O9	93.77(16)	93.10(18)	O2–Cu1–N1	91.69(11)
O3–M1–O7	86.37(15)	87.5(18)	O4–M2–O5	177.86(16)	177.1(2)	O3–Cu1–N2	92.96(12)
O7–M1–O9	89.85(15)	93.2(10)	O5–M2–O9	88.34(15)	88.53(18)	O2–C1–O1	123.0(3)
N1–M1–N2	84.40(19)	82.3(2)	N3–M2–N4	84.46(17)	82.1(2)	O3–C12–O4	122.3(3)
N1–M1–O1	87.05(16)	88.1(2)	N3–M2–O2	86.30(16)	87.4(2)	D1–Fe1–D2[c)]	178.5(3)
N1–M1–O3	86.04(18)	89.1(2)	N3–M2–O4	87.77(18)	82.1(2)	D3–Fe2–D4[c)]	176.5(3)
N1–M1–O7	90.43(17)	86.9(10)	N3–M2–O5	90.13(18)	88.6(2)		
N1–M1–O9	178.73(17)	178.8(2)	N3–M2–O9	178.24(18)	176.9(2)		
N2–M1–O1	89.51(17)	89.7(2)	N4–M2–O2	170.55(18)	169.2(2)		
N2–M1–O3	169.78(18)	169.9(2)	N4–M2–O4	89.97(17)	92.8(2)		
N2–M1–O7	90.10(17)	86.8(17)	N4–M2–O5	89.43(17)	89.4(2)		
N2–M1–O9	96.85(17)	98.8(2)	N4–M2–O9	96.40(16)	96.7(2)		
O1–C1–O2	127.1(5)	126.5(6)	O3–C12–O4	128.0(6)	126.6(6)		
O7–C34–O8	125.7(6)	126(3)	O5–C23–O6	123.8(6)	125.9(6)		

a) For **5A**/**6A** M1 and M2 refer to Ni1 and Ni2/Co1 and Co2, respectively. Of disordered units only data of one fragment are given. b) D1/D3/D5/D7 and D2/D4/D6/D8 denote geometrical centroids of C_5H_4 and C_5H_5 units, respectively. c) D1/D3 and D2/D4 denote geometrical centroids of C_5H_4 and C_5H_5 units, respectively.

The structure of ***7***: The molecular structure of **7** is displayed in Fig. 2 and selected bond lengths and angles are given in Table 1. The Cu atom of **7** is $\kappa^2 N,N'$-bonded by the tmeda and by two $\kappa^2 O,O'$-bonded O_2CFc ligands (Fig. 2). The thus formed CuN_2O_4 coordination unit exhibits a strongly distorted octahedral geometry, which might be better described as a distorted tetragonal-bipyramidal coordination geometry [66]. Related crystallographically described Cu^{II} coordination compounds of the general composition $[Cu(O_2CR)_2(N,N')]$ (R = organic group; *N*,*N*' = bidentate ligand with C_{sp3}–C_{sp3} bridges) [66–75] deposited with the CSD were used in for a structural comparison with **7**, as described in the SI. As a summary thereof it can be stated that **7** does not show structural peculiarities and compares well with its structural parameters to already described analogous coordination compounds.

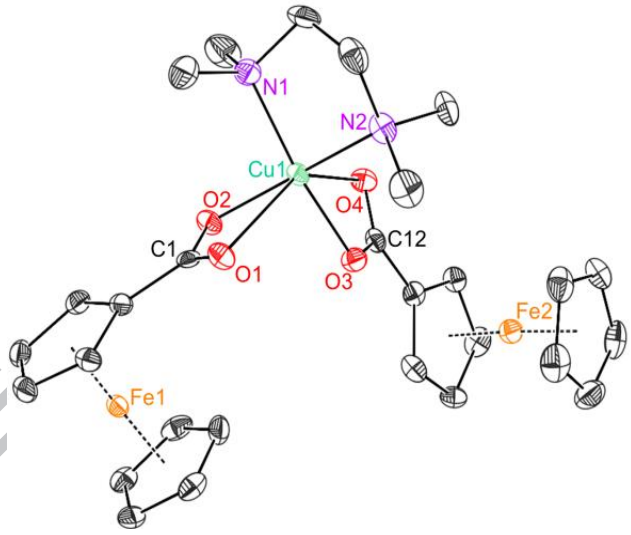

Fig. 2. ORTEP diagram (50 % ellipsoid probability) of the molecular structure of **7**. All hydrogen atoms were omitted for clarity. Iron to geometrical centroid distances of C_5H_4 and C_5H_5 units were indicated by dotted lines.

3.4. Thermogravimetric analysis

TG (= thermogravimetry) along with DSC (= differential scanning calorimetry) studies were carried out to determine the decomposition behaviour of **5** – **7** in the temperature range between 40 to 800 °C (Fig. S2, SI).

Hexanuclear **5** or **6** start to decompose at a significant lower temperatures (110 or 125 °C) when compared to trinuclear **7** (190 °C). The residual masses were determined to 18.5 (**5**), 21.2 (**6**) and 24.5 % (**7**). PXRD analysis (= X-ray powder diffraction) confirmed the formation of crystalline Fe_2O_3 (maghemit-Q; ICDD C00-039-1346) for all three compounds (Fig. S3, SI). The formation of Fe_2O_3 is attributed to traces of oxygen in the argon gas stream as discussed for **10** [12]]. Additionally, the formation of Fe_2O_3 under anaerobic conditions goes coherent with previously reported studies by Yilmaz et al. [76]. Beyond that, PXRD analysis reveal the formation of $FeNi_3$ (alloy, ICDD C01-071-8324) and $Fe_{0.64}Ni_{0.36}$ (alloy, ICDD C00-047-1405) for **5**, Co_3O_4 (ICDD C00-042-1467) and Fe (ICDD C00-006-0696) for **6**, and Cu_2O (cuprite; ICDD C00-005-0667) and $CuFeO_2$ (delafossite; ICDD C00-039-0246) for **7** (for more details see Fig. S3, SI).

3.5. Electrochemical properties

The redox properties of **5** – **7** have been investigated by cyclic voltammetry (CV) (25 °C) and square wave voltammetry (= SWV) (25 °C) (Fig. 3). As supporting electrolyte a 0.1 M solution of $[^nBu_4N][B(C_6F_5)_4]$ [77–91] in anhydrous dichloromethane was used. All redox potentials were referenced to the FcH/FcH^+ redox couple ($E°' = 0$ mV, FcH = $Fe(\eta^5\text{-}C_5H_5)_2$) [92]. The cyclic and square wave voltammograms are shown in Fig. 3 and data derived from CV measurements are summarized in Table 2. For simulation of the SWV potentials three or four Gaussian-shaped functions were applied to get fits well enough for an almost exact overlay with the experimental voltammograms (Table 2).

Within the cyclic voltammetry measurements of **5** two redox processes for the four ferrocenyl units were observed, whereas a third process is noticed as a shoulder. The difference between the cathodic and anodic peak potential (ΔE_p = 132 mV) for the first event at $E°'_1$ = 38 mV suggests two one electron processes in close potential proximity. In order to resolve the

ferrocenyl-based redox events deconvolution of the square wave voltammogram was performed (Fig. 3). The area ratio of the obtained four functions is 1:1.19:1.01:1.04, cf. Fig. 3, which corresponds to the subsequent oxidation of the ferrocenyls. Furthermore, the peak-to-peak separation of two superimposed one-electron processes within the cyclic voltammogram was determined by the method of Richardson and Taube [93]. For the 1st and 2nd redox process of **5** $\Delta E^{\circ\prime}$ was identified to be approximately 95 mV. This small potential difference is not resolved within standard cyclic voltammetry techniques.

For the ferrocenyl groups of **6** two redox events were observed within the CV. However, the asymmetric shape of the event at 270 – 360 mV emphasises that most probably more than one redox process takes place in a close potential range. The SWV for **6** shows four waves, whereby only the first one appears as a single one-electron process, while the following events were deconvoluted into three ferrocenyl-based partly superimposed oxidations (Fig. 3). Within the SWV an increased redox separation between the 1st and 2nd redox process of **6** compared to compound **5** ($\Delta E^{\circ\prime}$ = 86 mV, **5**; $\Delta E^{\circ\prime}$ = 209 mV, **6**) was found, indicating interactions between the Fc groups. In order to identify the origins of those interactions spectroelectrical measurements have been carried out. The UV-Vis/NIR spectroelectrochemical study of **6** (1.0 mmol·L^{-1} acetonitrile solution, 0.1 mol·L^{-1} of [^{n}Bu$_4$N][B(C$_6$F$_5$)$_4$] as supporting electrolyte) was performed in an OTTLE (= Optically Transparent Thin-Layer Electrochemical) cell [14]. During the measurements, oxidation of neutral **6** to mixed-valent [**6**]$^{+}$, and finally to the fully oxidized compounds [**6**]$^{4+}$ was performed by a stepwise increase of the potentials (step width: 25, 50, 100 mV, Fig. S6, SI). To prove the reversibility, **6** was reduced at −200mV after full oxidation and the afterwards measured UV-Vis/NIR spectrum was identical to the one of the starting compound. During the oxidation process (up to 1000 mV vs Ag^{+}/AgCl) no IVCT absorption (= inter-valence charge-transfer) were observed in the NIR region, indication that the large redox separation is caused mostly by electrostatic interactions between the Fc entities.

The two ferrocenyl groups in **7** oxidize separately ($E°'_1$ = 1 mV, $E°'_2$ = 171 mV). The differences between the cathodic and anodic peak potential ΔE_p of 70 and 78 mV indicate the reversible character of the ferrocenyl–based oxidations. The redox separation $\Delta E°'$ = 170 mV might be influenced by electrostatic interactions between the ferrocenyl units. In addition, a third process as a shoulder was observed at $E°'_3$ = 20 mV. Deconvolution of the SWV gave three redox processes of peak ratio 1:0.94:0.63. The 3rd event is most likely attributed to the oxidation of Cu^{II} which is in accordance with copper(II) carboxylates known to literature (–0.6 to 0.6 V) [94–98].

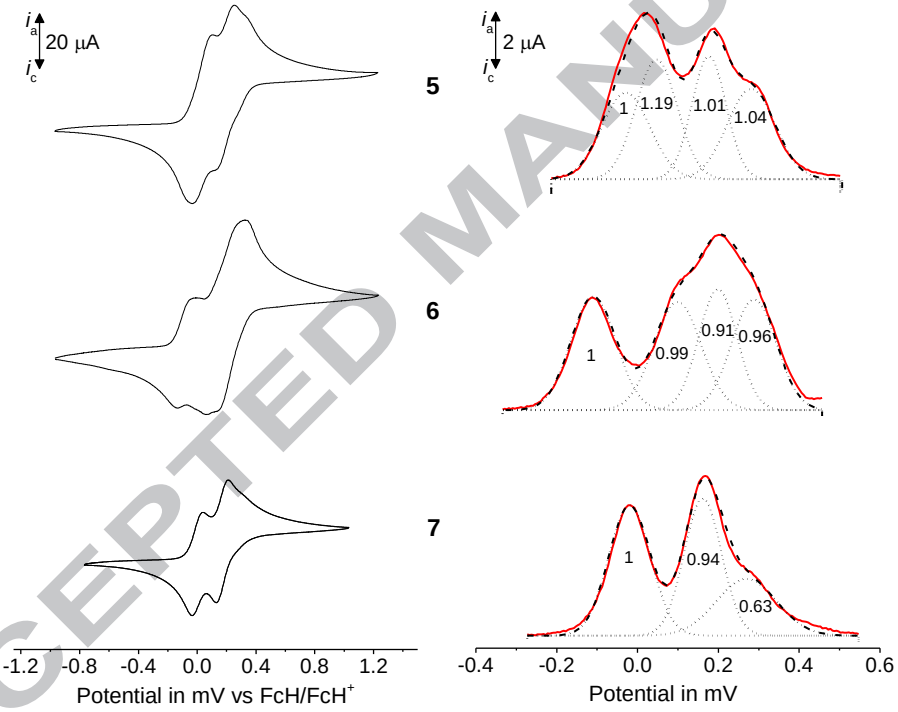

Fig. 3. Left: Cyclic voltammograms of **5** – **7** (1 mmol·L^{-1} dichloromethane solution, 25 °C, [^{n}Bu$_4$N][B(C$_6$F$_5$)$_4$] (0.1 mol·L^{-1}) as supporting electrolyte, scan rate = 100 mV s^{-1}). Right: Square wave voltammograms of **5** – **7** (0.1 mol·L^{-1} dichloromethane solution, 25 °C, [^{n}Bu$_4$N][B(C$_6$F$_5$)$_4$] (0.1 mol·L^{-1}) as supporting electrolyte, scan rate = 2.5 mV·s^{-1}) (red line). Spectral deconvolution of the SWVs was accomplished using Gaussian-shaped functions (dotted lines: individual electron transfer processes; dashed lines = sum of all electron transfer processes). All potentials are referenced to the [FcH]/[FcH]$^+$ redox couple.

Table 2. Cyclic and square-wave voltammetry data using three to four Gaussian-shaped functions for **5** – **7**.

	5				**6**				**7**		
Cyclic voltammetry data [a – d]											
$E°'_1$, V (ΔE_p, V)	0.02[g] (0.13)				–0.11 [g] (0.10)				0 (0.07)		
$E°'_2$, V (ΔE_p, V)	0.19[g] (0.13)				–[f]				0.17 (0.08)		
$E°'_3$, V (ΔE_p, V)	–[e]				0.20[g]				–[e]		
$\Delta E°'_1$, V	0.15				0.32[g]				0.17		
Square-wave voltammetry											
Process No.	**1**st	**2**nd	**3**rd	**4**th	**1**st	**2**nd	**3**rd	**4**th	**1**st	**2**nd	**3**rd
ratio	1	1.19	1.01	1.04	1	0.99	0.91	0.96	1	0.94	0.63
$E°'$ /V	–0.03	0.05	0.18	0.28	–0.11	0.10	0.20	0.29	–0.02	0.16	0.27
FWHM[h] /V	0.14	0.12	0.10	0.14	0.13	0.14	0.11	0.13	0.12	0.11	0.17

a) Potentials *vs* FcH/FcH^+, scan rate 100 $mV \cdot s^{-1}$ at glassy-carbon electrode of 1.0 $mmol \cdot L^{-1}$ solutions of **5** – **7** in dry dichloromethane; 0.1 $mol \cdot L^{-1}$ of $[^nBu_4N][B(C_6F_5)_4]$ as supporting electrolyte at 25 °C. b) ΔE_p = difference between anodic and cathodic peak potential ($\Delta E_p = E_{pa} - E_{pc}$). c) $E°'$ = formal potential ($E°' = E_{pa} + E_{pc})/2$). d) $\Delta E°'_1$ = difference between two redox processes ($\Delta E°' = E°'_2 - E°'_1$). e) $E_{pc/pa}$ values not possible to identify. Appears as a shoulder. f) E_{pc} value of second process not possible to identify, since second and third processes are superimposed. g) Determined from potentials of SWV measurements. h) Full Width of Half Maximum.

3.6. Magnetic measurements

Fig. 4 shows the product of the static magnetic susceptibility, corrected by the diamagnetic contribution of the ligands inferred from Pascal's constants [15], and temperature, $(\chi_{mol} - \chi_0)T$ (T), as well as the inverse susceptibility $1/(\chi_{mol} - \chi_0)$ (T) of **5** and **6**. For solids of **6**, at high temperatures, i.e. above T = 150 K, the data obey a Curie-Weiss-like behavior which is, e.g., shown by the fact that $(\chi_{mol} - \chi_0)T$ exhibits a constant value of $(\chi_{mol} - \chi_0)T$ = 5.85 erg K/G^2/mol. As temperature decreases, $(\chi_{mol} - \chi_0)T$ smoothly decreases, followed by a more steep decrease below around 17 K. At T = 2 K, it amounts to 0.99 erg K/G^2/mol. The low temperature decrease of $(\chi_{mol} - \chi_0)T$ observed for **6** can be either interpreted as signature of antiferromagnetic interaction between the Co^{II} moments or magnetic anisotropy of the metal ions.

Fitting the linear region of the inverse susceptibility (Fig. 4a) at T > 150 K by means of the Curie-Weiss law, i.e. $\chi_{mol} - \chi_0 = C/(T - \theta)$, yields the Curie constant C = 6.13 ± 0.01 erg K/G^2/mol and the Weiss temperature θ = –8.4 ± 0.4 K. The negative value of θ signals predominant antiferromagnetic coupling between the Co^{II} moments. Assuming Co^{II} being in

the high-spin configuration S = 3/2 allows extracting the g-factor from the Curie constant, i.e. $g = (\frac{8C}{nS(S+1)})^{1/2}$, which amounts to 2.55 ± 0.01.

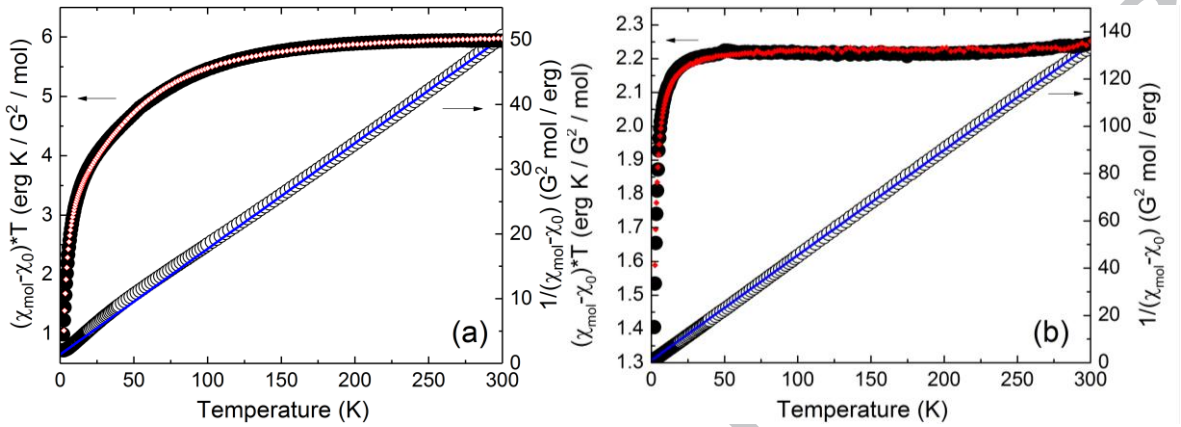

Fig. 4. Product of static magnetic susceptibility and temperature, (χ_{mol} - χ_0)T (T), and inverse susceptibility, 1/(χ_{mol} - χ_0) (T) of (a) **6** and (b) **5**. Black circles represent the experimental data. Blue lines show fits to the data by means of the Curie-Weiss law, and red diamonds show fits according to Hamiltonian Eq. 1 (see the text).

In order to determine the exchange interaction between the metal ions as well as the magnetic anisotropy, the data have been fitted using the julX simulation software package [99] according to the following Hamiltonian:

$$H = J\vec{S}_1 \cdot \vec{S}_2 + D_1 {S_{1,z}}^2 + D_2 {S_{2,z}}^2 + \mu_B g_1 \vec{B} \cdot \vec{S}_1 + \mu_B g_2 \vec{B} \cdot \vec{S}_2 \qquad \text{Eq. 1}$$

The first term is the exchange interaction term within the magnetic dimer with exchange integral, J, the second and third terms are the axial anisotropy terms with anisotropy constants, D. The fourth and fifth terms include the Zeeman energies for two individual Co^{II} moments. As shown in Fig. 5a, the simulation results are well matched to the experimental data with the parameters for **6** of J = 1.4 ± 0.02 cm^{-1}, g_1 = 2.53 ± 0.01, g_2 = 2.56 ± 0.01, $|D_1|$ = 63 ± 1 cm^{-1}, and $|D_2|$ = 58 ± 1 cm^{-1}. The obtained g-values are well matched to the ones from the Curie-Weiss analysis. While there is only a weak antiferromagnetic exchange of $J \approx 2$ K between the Co^{II} moments, a significant axial anisotropy is required to describe the data in terms of the Hamiltonian, Eq. 1. It can be ascribed to spin-orbit coupling which results in zero

field splitting and related depopulation of the ±3/2 doublet with respect to the ±1/2 one. Similar values are found in the literature for mononuclear high spin Co^{II} containing coordination compounds in distorted octahedral coordination environments where, e.g., g = 2.580, and $|D|$ = 87.9 cm^{-1},[100] or $|D|$ = 60(3) cm^{-1}, and g_z = 2.77(5), g_{xy} = 3.04(5) [101]. The slight discrepancy of g and D values between the two Co^{II} ions might be attributed to the observation of two crystallographic independent molecules of **6** in the solid state, namely **6A** and **6B** as described above.

Fig. 4b shows $(\chi_{mol} - \chi_0)T$ (T) and $1/(\chi_{mol} - \chi_0)T$ (T) of **5**. The $(\chi_{mol} - \chi_0)T$ data exhibit constant behavior with the amounts of 2.21 erg K/G^2/mol at high temperatures, i.e. in this case at T > 50 K. While the temperature scale is different from the finding for **6**, the qualitative behaviour is similar: χT smoothly decreases upon cooling but drops below 20 K to 1.4 erg K/G^2/mol at 2 K. Fitting the data at T > 100 K by means of the Curie-Weiss law provides C = 2.247 ± 0.004 erg K/G^2/mol and θ = –2.2 ± 0.3 K. The Curie constant implies S = 1 and g = 2.12 ± 0.005 which is slightly smaller than the often found g-values of Ni^{II} ions, g = 2.15 – 2.20 [102,103], but larger than g = 2.052 of Ni^{II} ions in binuclear coordination compound $[Ni_2(\mu\text{-}O_2P(H)Ant)_2(bpy)_4]Br_2$ [104]. The negative Weiss temperature again indicates predominant antiferromagnetic exchange interactions which is contradicting to a previous observation of weakly ferromagnetic behavior (θ = 1.6 K) observed for the similar species/compounds $[Ni_2(O_2CFcCO_2)_2(H_2O)(tmeda)_2]$ (**9**) [11]. The julX-fits [99] with the Hamiltonian, Eq. 1, yield a good description of the data, without including anisotropy terms, with the parameters J = 0.7 cm^{-1}, g_1 = 2.119 ± 0.002, and g_2 = 2.117 ± 0.002. The small value of $J \approx 1$ K again shows weak antiferromagnetic interaction between the two Ni^{II} moments. Note, that a similarly good description of the susceptibility data is possible by including $|D|$ up to 5 cm^{-1} and varying J accordingly, i.e. in the limits 0.1 $cm^{-1} \leq J \leq 0.3$ cm^{-1}. This would account for single ion anisotropy well established for Ni^{II} (cf., e.g., reference [103]). Typical values of

axial anisotropies of Ni^{II} ions in distorted octahedral environment obtained by high-frequency ESR measurements range from $D = -7.7$ cm^{-1} [105], –5.3 cm^{-1} [106], –3.2 cm^{-1} [107], –0.5 cm^{-1} [108] to $D = 1.875$ cm^{-1} [109] while in case of $[Ni_2(O_2CH)_4(H_2O)(tmeda)_2]$ (**10**) the magnetic anisotropy for the Ni^{II} ions is $D_{Ni,1} = 1.503$ cm^{-1} and $D_{Ni,2} = 1.83$ cm^{-1} [12], respectively.

Conclusion

Within this study, the synthesis of three discrete coordination compounds of type $[M_2(tmeda)_2(\mu^2\text{-}O_2CFc)_2(\eta^2\text{-}O_2CFc)_2(\mu^2\text{-}H_2O)]$ (M = Ni, **5**; Co, **6**) and $[Cu(tmeda)(O_2CFc)_2]$ (**7**) by the reaction of O_2CFc^- with the metal salts $[M(tmeda)(NO_3)_2]$ (M = Ni, **2**; Co, **3**; Cu, **4**) is reported. The structures of **5** – **7** in the solid state are presented, showing that **5** and **6** are isostructural. In **5** and **6** two M^{II} ions are bridged by two μ-O_2CFc^- building blocks and one μ-H_2O molecule. In contrast, in **7** the Cu^{II} ion is octahedrally surrounded by two asymmetric chelate-bonded $FcCO_2^-$ entities and one bidentate tmeda ligand. The thermal behaviour of **5** – **7** is discussed and decomposition afforded Fe_2O_3, $FeNi_3$ and $Fe_{0.64}Ni_{0.36}$ for **5**, Fe_2O_3, CoO and Fe for **6** and Fe_2O_3, Cu_2O and $CuFeO_2$ for **7** as evidenced by PXRD studies. Cyclic voltammetry measurements for **5** – **7** were performed showing that the number of Fc substituents corresponds to the number of redox events, however, in a close potential range. Within the square wave voltammograms the appropriate ferrocenyl oxidations were separated by using the method of deconvolution giving the expected four (**5**, **6**) or three (**7**) one-electron processes. Magnetic properties of **5** and **6** are characterized by weak antiferromagnetic exchange interaction between the magnetic centers, i.e. $J \approx 1$ K (**5**) and $J \approx 2$ K (**6**). No significant anisotropy is found for **5**. In contrast, the magnetic properties of **6** may be described by inferring uniaxial anisotropy of $D_1 = 63.3$ cm^{-1} and $D_2 = 58.1$ cm^{-1} for the two Co^{II} moments which accounts for spin-orbit coupling and distorted ligand cage.

Acknowledgments

We are grateful to the Deutsche Forschungsgemeinschaft (FOR 1154 "Towards Molecular Spintronics") for generous financial support. We thank Prof. Dr. M. Mehring and Dipl.-Chem. L. Mertens (TU Chemnitz) for PXRD measurements, Katrin Müller (TU Chemnitz) for elemental analysis, Brigitte Kempe as well as Dr. Roy Buschbeck (TU Chemnitz) for ESI-MS and Dipl.-Chem. Natalia Rüffer (TU Chemnitz) for TG measurements.

Appendix A. Supplementary data

CCDC 1547322 (**5'**), 1547331 (**6**), 1547330 (**7**) contains the supplementary crystallographic data for this paper. These data can be obtained free of charge via … , or from the Cambridge Crystallographic Data Centre, 12 Union Road, Cambridge CB2 1EZ UK; fax: (+44) 1223-336-033; or e-mail: deposite@ccdc.cam.ac.uk.

Supplementary data associate with this article can be found, in the online version, at …

References

[1] M.N. Baibich, J.M. Broto, A. Fert, F. Nguyen Van Dau, F. Petroff, P. Eitenne, G. Creuzet, A. Friederich, J. Chazelas, Phys. Rev. Lett. 61 (1988) 2472–2475.

[2] G. Binasch, P. Grünberg, F. Saurenbach, W. Zinn, Phys. Rev. B 39 (1989) 4828–4830.

[3] P. Grünberg, R. Schreiber, Y. Pang, U. Walz, M.B. Brodsky, H. Sowers, J. Appl. Phys. 61 (1987) 3750–3752.

[4] J. Barnaś, A. Fuss, R.E. Camley, P. Grünberg, W. Zinn, Phys. Rev. B 42 (1990) 8110–8120.

[5] S. Sanvito, Chem. Soc. Rev. 40 (2011) 3336–3355.

[6] U. Pfaff, A. Hildebrandt, M. Korb, S. Oßwald, M. Linseis, K. Schreiter, S. Spange, R.F. Winter, H. Lang, Chem. - A Eur. J. 22 (2016) 783–801.

[7] S.J. Matthäus, M. Korb, A. Schade, S. Spange, H. Lang, Organometallics 34 (2015) 3788–3798.

[8] D. Miesel, A. Hildebrandt, M. Korb, D.A. Wild, P.J. Low, H. Lang, Chem. - A Eur. J. 21 (2015) 11545–11559.

[9] E.A. Poppitz, M. Korb, H. Lang, Acta Crystallogr. Sect. E Struct. Reports Online 70 (2014) 238–241.

[10] A. Hildebrandt, H. Lang, Organometallics 32 (2013) 5640–5653.

[11] J. Kühnert, T. Rüffer, P. Ecorchard, B. Bräuer, Y. Lan, A.K. Powell, H. Lang, Dalton Trans. (2009) 4499–4508.

[12] K. Rühlig, A. Abylaikhan, A. Aliabadi, V. Kataev, S. Liebing, S. Schwalbe, K. Trepte, C. Ludt, J. Kortus, B. Büchner, T. Rüffer, H. Lang, Dalt. Trans. 46 (2017) 3963–3979.

[13] M.D. Rausch, D.J. Ciappenelli, J. Organomet. Chem. 10 (1967) 127–136.

[14] M. Krejčik, M. Daněk, F. Hartl, J. Electroanal. Chem. 317 (1991) 179–187.

[15] G.A. Bain, J.F. Berry, J. Chem. Educ. 85 (2008) 532.

[16] G.M. Sheldrick, Acta Cryst A64 (2008) 112–122.

[17] K. Nakamoto, Infrared and Raman Spectra of Inorganic and Coordination Compounds Part B: Applications in Coordination, Organometallic, and Bioinorganic Chemistry, 6th ed., John Wiley & Sons, Hoboken, New Jersey, 2009.

[18] G.B. Deacon, R.J. Phillips, Coord. Chem. Rev. 33 (1980) 227–250.

[19] U. Turpeinen, R. Hämäläinen, Polyhedron 6 (1987) 1603–1610.

[20] B. Ye, I.D. Williams, X. Li, J. Inorg. Biochem. 92 (2002) 128–136.

[21] S.B. Yu, S.J. Lippard, I. Shweky, A. Bino, Inorg. Chem. 31 (1992) 3502–3504.

[22] H. Günzler, H.-U. Gremlich, IR-Spektroskopie, 4th ed., Wiley-VCH, Weinheim, 2003.

[23] L.J. Bellamy, A.J. Owen, Spectrochim. Acta 25A (1969) 329–333.

[24] S. Singh, D. Saini, S.K. Mehta, D. Choquesillo-Lazarte, J. Coord. Chem. 64 (2011) 1544–1553.

[25] M. Ahlgren, R. Hämäläinen, U. Turpeinen, Cryst. Struct. Commun 6 (1977) 829–834.

[26] G. Dong, L. Yu-ting, D. Chun-ying, M. Hong, M. Qing-jin, Inorg. Chem. 42 (2003) 2519–2530.

[27] W.-D. Song, J.-B. Yan, X.-M. Hao, Acta Crystallogr. Sect. E 64 (2008) m919–m920.

[28] M. Ahlgren, U. Turpeinen, Acta Cryst. B38 (1982) 276–279.

[29] M. Ahlgren, U. Turpeinen, R. Hämäläinen, Acta Chem. Scand. A32 (1978) 189–194.

[30] M. Ahlgren, U. Turpeinen, Acta Crystallogr. Sect. B B38 (1982) 276–279.

[31] S. Kennedy, G. Karotsis, C.M. Beavers, S.J. Teat, E.K. Brechin, S.J. Dalgarno, Angew. Chemie Int. Ed. 49 (2010) 4205–4208.

[32] A. Pons-Balague, S. Pilikos, S.J. Teat, S.J. Costa, M. Shiddiq, S. Hill, G.R. Castro, P. Ferrer-Escorihuela, E.C. Sanudo, Chem.-Eur. J. 19 (2013) 9064–9071.

[33] A. Karmakar, R.J. Sarma, J.B. Baruah, Eur. J. Inorg. Chem. 2006 (2006) 4673–4678.

[34] U. Turpeinen, Finn. Chem. Lett. (1976) 173–178.

[35] A. Karmakar, K. Deka, R.J. Sarma, J.B. Baruah, Inorg. Chem. Commun. 9 (2006) 836–838.

[36] C.H.L. Kennard, E.J. O'Reilly, G. Smith, Polyhedron 3 (1984) 689–693.

[37] O.T. Denisova, G.G. Aleksandrov, O.P. Fialkovskii, S.E. Nefedov, Russ. J. Inorg. Chem. 48 (2003) 1476.

[38] X.-M. Li, Q.-W. Wang, B. Liu, Z.-T. Wang, Chiniese J. Inorg. Chem. 26 (2010) 1904–1907.

[39] U. Turpeinen, Finn. Chem. Lett. (1977) 36–41.

[40] I.L. Eremenko, S.E. Nefedov, A.A. Sidorov, M.A. Golubnichaya, P. V. Danilov, V.N. Ikorskii, Y.G. Shvedenkov, V.M. Novotortsev, I.I. Moiseev, Inorg. Chem. 38 (1999) 3764–3773.

[41] A.M. Qadir, Asian J. Chem. 25 (2013) 8829–8830.

[42] J. Hudák, R. Boča, J. Moncol, J. Titiš, Inorganica Chim. Acta 394 (2013) 401–409.

[43] D. Guo, H. Mo, X.-Y. Tu, C.-Y. Duan, Q.-J. Meng, Chinese J. Chem. 19 (2003) 54–58.

[44] D.A. Brown, W.K. Glass, N.J. Fitzpatrick, T.J. Kemp, W. Errington, G.J. Clarkson, W. Haase, F. Karsten, A.H. Mahdy, Inorganica Chim. Acta 357 (2004) 1411–1436.

[45] B.-Y. Zhang, T.-G. Xu, D.-J. Xu, Acta Crystallogr. Sect. E Struct. Reports Online 62 (2006) m2186–m2188.

[46] J.C. Burley, T.J. Prior, Acta Crystallogr. Sect. E Struct. Reports Online 61 (2005) m1422–m1424.

[47] R.W. Corkery, D.C.R. Hockless, Acta Crystallogr. Sect. C Cryst. Struct. Commun. 53 (1997) 840–843.

[48] M.A. Golubnichaya, A.A. Sidorov, I.G. Fomina, L.T. Eremenko, S.E. Nefedov, I.L. Eremenko, I.I. Moiseev, Russ. J. Inorg. Chem. 44 (1999) 1401–1410.

[49] A.P. Gulya, S.G. Shova, G. V. Novitsky, M.D. Mazus, Koord.Khim.(Russ.)(Coord. Chem.) 20 (1994) 110–115.

[50] K.S. Hagen, R. Lachicotte, A. Kitaygorodskiy, A. Elbouadili, Angew. Chem. Int. Ed. 32 (1993) 1321–1324.

[51] A. Karmakar, R.J. Sarma, J.B. Baruah, Polyhedron 26 (2007) 1347–1355.

[52] A. Karmakar, R.J. Sarma, J.B. Baruah, Eur. J. Inorg. Chem. 2007 (2007) 643–647.

[53] L.-L. Kong, L.-H. Huo, S. Gao, J.-G. Zhao, Acta Crystallogr. Sect. E Struct. Reports

Online 61 (2005) m2485–m2487.

[54] C.-S. Liu, J.-J. Wang, L.-F. Yan, Z. Chang, X.-H. Bu, E.C. Sanudo, J. Ribas, Inorg. Chem. 46 (2007) 6299–6310.

[55] Q. Miao, M.-L. Hu, F. Chen, Acta Crystallogr. Sect. E Struct. Reports Online 60 (2004) m1314–m1316.

[56] F.P. Pruchnik, U. Dawid, A. Kochel, Polyhedron 25 (2006) 3647–3652.

[57] G.G. Sadikov, A.S. Antsyshkina, T. V. Koksharova, I.S. Gritsenko, V.S. Sergienko, Crystallogr. Reports 52 (2007) 819–825.

[58] M.A. Uvarova, E.V. Kushan, M.V. Andreev, A.O. Voroshilina, S.E. Nefedov, Zh.Neorg.Khim.(Russ.)(Russ.J.Inorg.Chem.) 57 (2012) 1232–1243.

[59] Q.-W. Wang, X.-M. Li, Z.-T. Wang, B. Liu, Chin. J. Struct. Chem. 29 (2010) 1814–1817.

[60] B.-H. Ye, X.-M. Chen, Chinese J. Chem. 21 (2003) 531–536.

[61] B.-S. Zhang, C.-S. Wu, Y.-H. Wang, Chin. J. Struct. Chem. 27 (2008) 1360–1364.

[62] S.-H. Zhang, Y.-Q. Yang, W. Li, Chin. J. Struct. Chem. 31 (2012) 1681–1684.

[63] I. Zimmermann, T.D. Keene, A. Neels, S. Decurtins, Acta Crystallogr. Sect. E 64 (2008) m845-6.

[64] Z.P. Zubreichuk, O.. Denisova, V.A. Knizhnikov, S.E. Nefedov, Russ. Chem. Bull. 53 (2004) 1701–1703.

[65] U. Turpeinen, M. Ahlgren, R. Hämäläinen, Finn. Chem. Lett. (1977) 246–251.

[66] D. Mikloš, P. Segl'a, M. Palicová, M. Kopcová, M. Melník, M. Valko, T. Glowiak, M. Korabik, J. Mrozinski, Polyhedron 20 (2001) 1867–1874.

[67] N. Sanjeevakumar, M. Periasamy, Tetrahedron: Asymmetry 20 (2009) 1842–1847.

[68] S. Singh, J. Chaturvedi, S. Bhattacharya, Dalt. Trans. 41 (2012) 424–431.

[69] M. Ahlgren, U. Turpeinen, R. Hämäläinen, Acta Chem. Scand. A 34 (1980) 67–70.

[70] M. Ahlgren, R. Hämäläinen, U. Turpeinen, Acta Chem. Scand. A32 (1978) 57–61.

[71] H. Muhonen, R. Hämäläinen, Acta Crystallogr. Sect. B 34 (1978) 1842–1846.

[72] J.C. Slootweg, P. Chen, Acta Crystallogr. Sect. E 64 (2008) m430–m431.

[73] L. Ponikiewski, A. Rothenberger, Inorganica Chim. Acta 361 (2008) 43–48.

[74] L. Ponikiewski, A. Rothenberger, Inorganica Chim. Acta 358 (2005) 1322–1326.

[75] L. Parkanyi, G. Speier, Zeitschrift Für Krist. 210 (1995) 307–308.

[76] V.T. Yilmaz, A. Karadag, H. Icbudak, Thermochim. Acta 261 (1995) 107–118.

[77] R.J. LeSuer, C. Buttolph, W.E. Geiger, Anal. Chem. 76 (2004) 6395–6401.

[78] F. Barrière, W.E. Geiger, J. Am. Chem. Soc 128 (2006) 3980–3989.

[79] H. Strehlow, W. Knoche, H. Schneider, Ber. Bunsenges. Phys. Chem. 77 (1973) 760–771.

[80] A. Hildebrandt, H. Lang, Dalt. Trans. 40 (2011) 11831–11837.

[81] D. Miesel, A. Hildebrandt, M. Korb, P.J. Low, H. Lang, Organometallics 32 (2013) 2993–3002.

[82] U. Pfaff, A. Hildebrandt, D. Schaarschmidt, T. Rüffer, P.J. Low, H. Lang,

Organometallics 32 (2013) 6106–6117.

[83] A. Hildebrandt, H. Lang, Organometallics 32 (2013) 5640–5653.

[84] A. Hildebrandt, D. Schaarschmidt, R. Claus, H. Lang, Inorg. Chem. 50 (2011) 10623–10632.

[85] A. Hildebrandt, D. Schaarschmidt, H. Lang, Organometallics 30 (2011) 556–563.

[86] V.N. Nemykin, G.T. Rohde, C.D. Barrett, R.G. Hadt, C. Bizzarri, P. Galloni, B. Floris, I. Nowik, R.H. Herber, A.G. Marrani, R. Zanoni, N.M. Loim, J. Am. Chem. Soc 131 (2009) 14969–14978.

[87] V.N. Nemykin, G.T. Rohde, C.D. Barrett, R.G. Hadt, J.R. Sabin, G. Reina, P. Galloni, B. Floris, Inorg. Chem. 49 (2010) 7497–7509.

[88] D. Chong, J. Slote, W.E. Geiger, J. Electroanal. Chem. 630 (2009) 28–34.

[89] J.C. Swarts, A. Nafady, J.H. Roudebush, S. Trupia, W.E. Geiger, Inorg. Chem. 48 (2009) 2156–2165.

[90] E. Fourie, J.C. Swarts, D. Lorcy, N. Bellec, Inorg. Chem. 49 (2010) 952–959.

[91] H.J. Gericke, N.I. Barnard, E. Erasmus, J.C. Swarts, M.J. Cook, M.A.S. Aquino, Inorg. Chim. Acta 363 (2011) 2222–2232.

[92] G. Gritzner, J. Kuta, Pure Appl. Chem. 56 (1984) 461–466.

[93] D.E. Richardson, H. Taube, Inorg. Chem. 20 (1981) 1278–1285.

[94] M. Iqbal, I. Ahmad, S. Ali, N. Muhammad, S. Ahmed, M. Sohail, Polyhedron 50 (2013) 524–531.

[95] R. Ruiz, C. Surville-Barland, A. Aukauloo, E. Anxolabehere-Mallart, Y. Journaux, J. Cano, M.C. Muñoz, J. Chem. Soc. Dalt. Trans. (1997) 745–752.

[96] B. Cervera, J.L. Sanz, M.J. Ibáñez, G. Vila, F. LLoret, M. Julve, R. Ruiz, X. Ottenwaelder, A. Aukauloo, S. Poussereau, Y. Journaux, M.C. Muñoz, J. Chem. Soc. Dalt. Trans. (1998) 781–790.

[97] E. Pardo, J. Ferrando-Soria, M.C. Dul, R. Lescouëzec, Y. Journaux, R. Ruiz-García, J. Cano, M. Julve, F. Lloret, L. Cañadillas-Delgado, J. Pasán, C. Ruiz-Pérez, Chem. - A Eur. J. 16 (2010) 12838–12851.

[98] J. Soto, R. Martínez-Máñez, J. Payá, F. Lloret, M. Julve, 18 (1993) 69–72.

[99] Http://www.mpibac.mpg.de/bac/index_en.php/logins/bill/julX_en.php, (n.d.).

[100] J.W. Shin, S.R. Rowthu, M.Y. Hyun, Y.J. Song, C. Kim, B.G. Kim, K.S. Min, Dalt. Trans. 40 (2011) 5762.

[101] R.A. Polunin, N.P. Burkovskaya, J.A. Satska, S. V. Kolotilov, M.A. Kiskin, G.G. Aleksandrov, O. Cador, L. Ouahab, I.L. Eremenko, V. V. Pavlishchuk, Inorg. Chem. 54 (2015) 5232.

[102] J. Krzystek, A. Ozarowski, Telser, J. Coord. Chem. Rev. 250 (2006) 2308.

[103] Y. Krupskaya, A. Alfonsov, A. Parameswaran, V. Kataev, R. Klingeler, G. Steinfeld, N. Beyer, M. Gressenbuch, B. Kersting, B. Büchner, Chem. Phys. Chem. 11 (2010) 1961–1970.

[104] D. Yakhvarov, E. Trofimova, O. Sinyashin, O. Kataeva, Y. Budnikova, P. Lönnecke, E. Hey-Hawkins, A. Petr, Y. Krupskaya, V. Kataev, R. Klingeler, B. Büchner, Inorg. Chem. 50 (2011) 4553–4558.

[105] C. Mennerich, H.-H. Klauss, M. Broekelmann, F.J. Litterst, C. Golze, R. Klingeler, V. Kataev, B. Büchner, S.-N. Grossjohann, W. Brenig, M. Goiran, H. Rakoto, J.-M. Broto, O. Kataeva, D.J. Price, Phys. Rev. B 73 (2006) 174415.

[106] E.-C. Yang, C. Kirman, J. Lawrence, L.N. Zakharov, A.L. Rheingold, S. Hill, D.N. Hendrickson, Inorg. Chem. 44 (2005) 382.

[107] C. Golze, A. Alfonsov, R. Klingeler, B. Büchner, V. Kataev, C. Mennerich, H.-H. Klauss, M. Goiran, J.-M. Broto, H. Rakoto, S. Demeshko, G. Leibeling, F. Meyer, Phys. Rev. B 73 (2006) 224403/1-8.

[108] M. Golecki, J. Lach, A. Jeremies, F. Lungwitz, M. Fronk, G. Salvan, D.R.T. Zahn, J. Park, Y. Krupskaya, V. Kataev, R. Klingeler, B. Büchner, B. Mahns, M. Knupfer, P.F. Siles, O.G. Schmidt, A. Reis, W.R. Thiel, D. Breite, B. Abel, B. Kersting, Chem. Eur. J. 19 (2013) 7787–7801.

[109] L.A. Pardi, A.K. Hassan, F.B. Hulsbergen, J. Reedijk, A.L. Spek, L.-C. Brunel, Inorg. Chem. 39 (2000) 159.

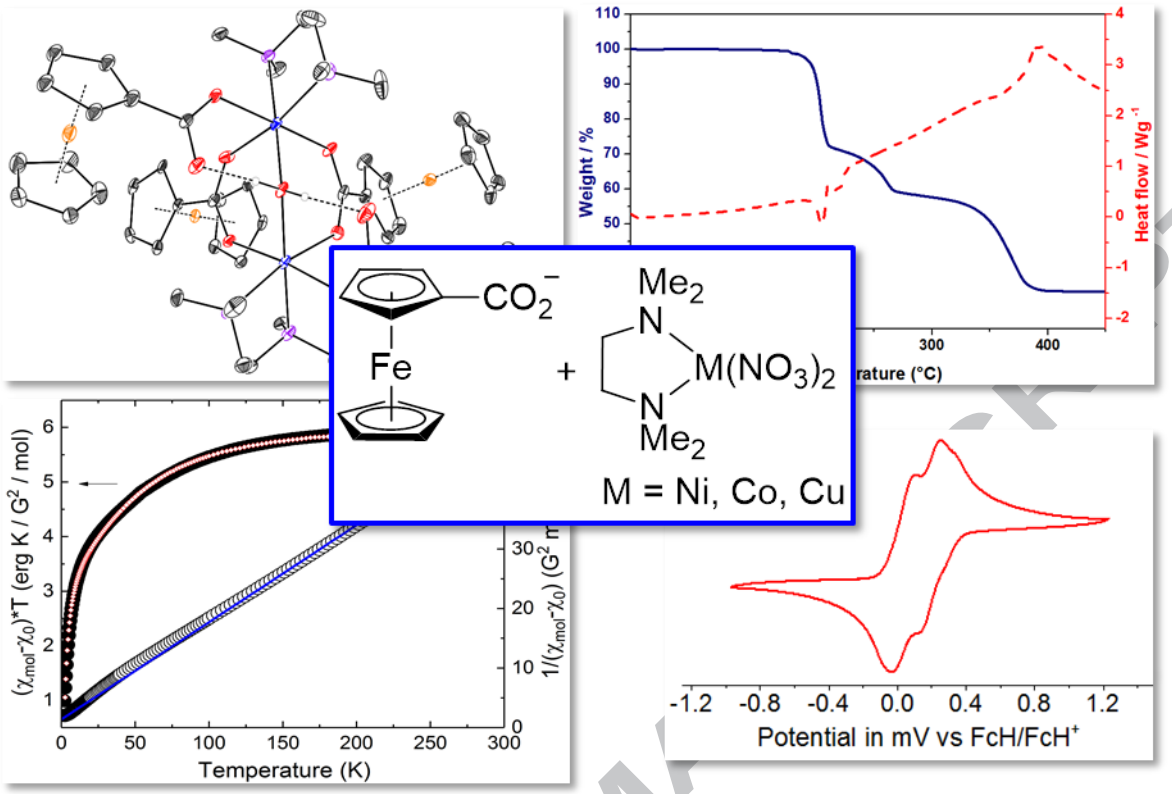

The trinuclear complex [Cu(tmeda)(O_2CFc)$_2$] (**7**) and the two hexanuclear complexes [M_2(O_2CFc)$_2$(μ-O_2CFc)$_2$(μ-H_2O)(tmeda)$_2$] (M = Ni, **5**; Co, **6**) are shown to undergo reversible redox events according to their number of ferrocenyl substituents. Susceptibility measurements revealed for **5** and **6** a weak antiferromagnetism while **6** shows additionally an uniaxial anisotropy.